An efficient numerical method for evolving microstructures with strong elastic inhomogeneity

2015 Modelling Simul. Mater. Sci. Eng. 23 045007

(http://iopscience.iop.org/0965-0393/23/4/045007)

IOP Publishing Modelling and Simulation in Materials Science and Engineering

Modelling Simul. Mater. Sci. Eng. **23** (2015) 045007 (13pp) doi:10.1088/0965-0393/23/4/045007

An efficient numerical method for evolving microstructures with strong elastic inhomogeneity

Darae Jeong[1], Seunggyu Lee[1] and Junseok Kim[1,2]

[1] Department of Mathematics, Korea University, Seoul 136-713, Republic of Korea

E-mail: cfdkim@korea.ac.kr

Received 14 January 2015
Accepted for publication 20 March 2015
Published 20 April 2015

Abstract

In this paper, we consider a fast and efficient numerical method for the modified Cahn–Hilliard equation with a logarithmic free energy for microstructure evolution. Even though it is physically more appropriate to use a logarithmic free energy, a quartic polynomial approximation is typically used for the logarithmic function due to a logarithmic singularity. In order to overcome the singularity problem, we regularize the logarithmic function and then apply an unconditionally stable scheme to the Cahn–Hilliard part in the model. We present computational results highlighting the different dynamic aspects from two different bulk free energy forms. We also demonstrate the robustness of the regularization of the logarithmic free energy, which implies the time-step restriction is based on accuracy and not stability.

Keywords: Cahn–Hilliard equation, logarithmic free energy, phase-field method, elastic inhomogeneity, unconditionally gradient stable scheme, multigrid

(Some figures may appear in colour only in the online journal)

1. Introduction

Elastic strain energy can be generated during a solid-state phase transformation and it is important in determining the transformation path and the corresponding microstructure evolution [1]. The microscopic phase-field model was created by Khachaturyan [2] and developed by Chen *et al* [3–6]. The model describes the spatial distribution of chemical species by atom occupation probability based on Onsager and Ginzburg–Landau theory. Many approaches have been proposed for modeling the elastic effect on precipitate morphology with a significant elastic inhomogeneity [7–12]. The main purpose of this paper is to present a fast and efficient numerical

[2] http://math.korea.ac.kr/cfdkim/

method for the modified Cahn–Hilliard (CH) equation with a logarithmic free energy for the two-dimensional microstructure evolution with strong elastic inhomogeneity:

$$\frac{\partial c}{\partial t} = M\Delta\mu, \tag{1}$$

$$\mu = \frac{\mathrm{d}F_{\mathrm{ch}}}{\mathrm{d}c} + \frac{\partial F_{\mathrm{el}}}{\partial c} - \epsilon^2\Delta c, \tag{2}$$

where $c = c(x, y, t)$ is the mole fraction at position (x, y) and time t. M is a mobility, $F_{\mathrm{ch}}(c)$ is the chemical energy density, $F_{\mathrm{el}}(c, \mathbf{u})$ is the elastic energy density, $\mathbf{u} = (u(x, y), v(x, y))$ is the displacement and ϵ is the gradient energy coefficient [13, 14]. The original logarithmic chemical energy density F_{ch} [15] is given as

$$F_{\mathrm{ch}}^{\log} = \frac{\theta}{2}[c\ln c + (1-c)\ln(1-c)] + \theta_{\mathrm{c}}c(1-c), \tag{3}$$

where θ and θ_{c} are temperature and critical temperature, respectively. Even though it is physically more appropriate to use the logarithmic free energy, a quartic polynomial approximation is typically used for the logarithmic function due to a logarithmic singularity. Many researchers [16–23] have used a quartic polynomial

$$F_{\mathrm{ch}}^{\mathrm{poly}}(c) = 2.5(c - c_{\mathrm{eq}}^{\alpha})^2(c - c_{\mathrm{eq}}^{\beta})^2 \tag{4}$$

as a substitute for the original logarithmic free energy $F_{\mathrm{ch}}^{\log}$ since the polynomial approximation is much easier to deal with numerically. Here, c_{eq}^{α}, c_{eq}^{β} are two local minima. For example, the derivatives of the logarithmic energy function have singular points at 0 and 1. To overcome the numerical difficulties associated with the original logarithmic free energy function, we employ a regularization procedure for the logarithmic free energy [24]:

$$F_{\delta}^{\log}(c) \coloneqq \begin{cases} \dfrac{\theta}{2}\left[c\ln(\delta) + (1-c)\ln(1-c) + \dfrac{c^2}{2\delta} - \dfrac{\delta}{2}\right] + \theta_{\mathrm{c}}c(1-c) & \text{if } c \leqslant \delta, \\ \dfrac{\theta}{2}\left[c\ln c + (1-c)\ln(\delta) + \dfrac{(1-c)^2}{2\delta} - \dfrac{\delta}{2}\right] + \theta_{\mathrm{c}}c(1-c) & \text{if } c \geqslant 1-\delta, \\ F_{\mathrm{ch}}^{\log}(c) & \text{otherwise,} \end{cases} \tag{5}$$

where $\delta(< c_{\mathrm{eq}}^{\alpha})$ is a small positive number. $F_{\mathrm{ch}}^{\mathrm{poly}}(c)$ and the regularized free energy $F_{\delta}^{\log}(c)$ are shown in figure 1.

The elastic energy density has the following form

$$F_{\mathrm{el}}(c, \mathbf{u}) = -(C_{11} + C_{12})e(c)(E_{11} + E_{22} - e(c)) + 2C_{44}E_{12}^2 + 0.5C_{11}(E_{11}^2 + E_{22}^2) + C_{12}E_{11}E_{22},$$

where C_{11}, C_{12} and C_{44} are the cubic elastic parameters and are dependent on the order parameter c. Here, $C_k = C_k^{\mathrm{l}}c + C_k^0(1-c)$ for $k = 11$, 12 and 44, where C_k^0 and C_k^{l} are elastic constants of matrix and precipitate, respectively. The eigenstrain is $e(c) = \eta(c - c_s)$, which obeys Vegard's law. Here, c_s is the average composition and η is a constant.

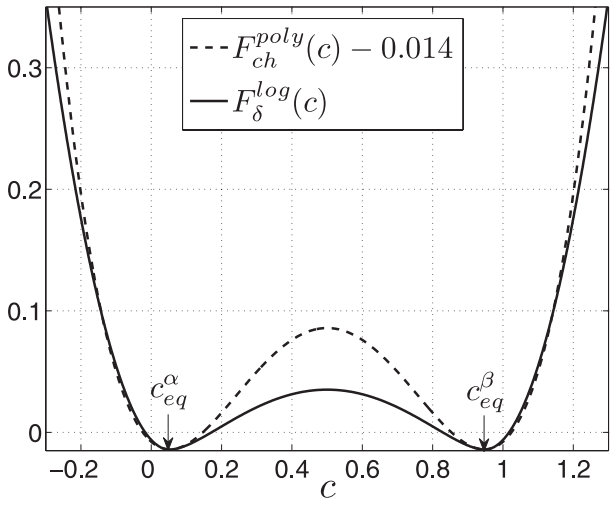

Figure 1. Chemical energy densities: $F_{\mathrm{ch}}^{\mathrm{poly}}(c)$ and $F_{\delta}^{\mathrm{log}}(c)$ with $\theta = 0.62$, $\theta_{\mathrm{c}} = 1$ and $\delta = 0.04$. The local minima are approximately $c_{\mathrm{eq}}^{\alpha} = 0.053$ and $c_{\mathrm{eq}}^{\beta} = 0.947$. Here, we plot $F_{\mathrm{ch}}^{\mathrm{poly}}(c) - 0.014$ for a comparison reason.

$$E_{ij} = \frac{1}{2}\left(\frac{\partial u_i}{\partial x_j} + \frac{\partial u_j}{\partial x_i}\right), \qquad \text{for } i,j = 1,2, \tag{6}$$

where $u_1 = u$, $u_2 = v$, $x_1 = x$ and $x_2 = y$. From the definition, we get

$$\begin{aligned}\frac{\partial F_{\mathrm{el}}}{\partial c} = &-(C_{11}^{\mathrm{l}} - C_{11}^{0} + C_{12}^{\mathrm{l}} - C_{12}^{0})e(c)(E_{11} + E_{22} - e(c)) \\ &-\eta(C_{11} + C_{12})(E_{11} + E_{22} - 2e(c)) + 2(C_{44}^{\mathrm{l}} - C_{44}^{0})E_{12}^{2} \\ &+0.5(C_{11}^{\mathrm{l}} - C_{11}^{0})(E_{11}^{2} + E_{22}^{2}) + (C_{12}^{\mathrm{l}} - C_{12}^{0})E_{11}E_{22}.\end{aligned} \tag{7}$$

Under the condition for plain strain and the quasi-static approximation, we have

$$(C_{11}u_x + C_{12}v_y)_x + (C_{44}u_y + C_{44}v_x)_y = [(C_{11} + C_{12})e(c)]_x, \tag{8}$$

$$(C_{11}v_y + C_{12}u_x)_y + (C_{44}v_x + C_{44}u_y)_x = [(C_{11} + C_{12})e(c)]_y, \tag{9}$$

where the subscripts, x and y, denote partial derivatives with respect to the corresponding arguments.

This paper is organized as follows. In section 2, we describe the numerical method used to solve the Cahn–Hilliard equation with elasticity term. To show the efficiency of the scheme, numerical examples are presented in section 3. Lastly, conclusions are drawn in section 4.

2. Numerical solutions

In this section, we present fully discrete schemes for the CH equations and the displacement equation. Let $N_x$and N_y be positive even integers, $h = L_1/N_x = L_2/N_y$ be the uniform mesh size and Ω_h=$\{(x_i, y_j)$: $x_i = (i - 0.5)h$, $y_j = (j - 0.5)h$, $1 \leqslant i \leqslant N_x$, $1 \leqslant j \leqslant N_y$ $\}$ be the set of cell-centers. Let c_{ij}, μ_{ij}, u_{ij} and v_{ij} be approximations of $c(x_i, y_j)$, $\mu(x_i, y_j)$, $u(x_i, y_j)$ and $v(x_i,$

y_j), respectively. Periodic boundary conditions are applied along both axes. We use the non-linearly stabilized splitting scheme [25, 26] for c in equations (1) and (2) as

$$\frac{c_{ij}^{n+1}-c_{ij}^{n}}{\Delta t}=\Delta_d \mu_{ij}^{n+\frac{1}{2}}, \tag{10}$$

$$\mu_{ij}^{n+\frac{1}{2}}=\frac{\mathrm{d}F_{\mathrm{ch}}^{\mathrm{C}}(c_{ij}^{n+1})}{\mathrm{d}c}+\frac{\mathrm{d}F_{\mathrm{ch}}^{\mathrm{E}}(c_{ij}^{n})}{\mathrm{d}c}-\epsilon^2\Delta_d c_{ij}^{n+1}+\frac{\partial F_{\mathrm{el}}(c_{ij}^{n},\mathbf{u}_{ij}^{n})}{\partial c}, \tag{11}$$

where $F_{\mathrm{ch}}^{\mathrm{C}}(c^{n+1})$ and $F_{\mathrm{ch}}^{\mathrm{E}}(c^{n})$ denote contractive and expansive parts of F_{ch}, respectively. By the regularized logarithmic free energy $F_{\delta}^{\log}(c)$, we define the two parts as follows.

$$\frac{\mathrm{d}F_{\mathrm{ch}}^{\mathrm{C}}(c_{ij}^{n+1})}{\mathrm{d}c}:=\begin{cases}\dfrac{\theta}{2}\left[\dfrac{c^{n+1}-\delta}{\delta}+\ln\left(\dfrac{\delta}{1-c^{n+1}}\right)\right] & \text{if } c^{n+1}\leqslant\delta,\\[2ex] \dfrac{\theta}{2}\left[\ln\left(\dfrac{c^{n+1}}{\delta}\right)-\dfrac{1-c^{n+1}-\delta}{\delta}\right] & \text{if } c^{n+1}\geqslant 1-\delta,\\[2ex] \dfrac{\theta}{2}\ln\left(\dfrac{c^{n+1}}{1-c^{n+1}}\right) & \text{otherwise.}\end{cases} \tag{12}$$

$$\frac{\mathrm{d}F_{\mathrm{ch}}^{\mathrm{E}}(c_{ij}^{n})}{\mathrm{d}c}:=-2\theta_{\mathrm{c}}c^{n}. \tag{13}$$

For the given polynomial energy density (4), we use the following equations:

$$\frac{\mathrm{d}F_{\mathrm{ch}}^{\mathrm{C}}(c^{n+1})}{\mathrm{d}c}=10\left(c_{ij}^{n+1}-\frac{c_{\mathrm{eq}}^{\alpha}+c_{\mathrm{eq}}^{\beta}}{2}\right)^3, \tag{14}$$

$$\frac{\mathrm{d}F_{\mathrm{ch}}^{\mathrm{E}}(c^{n})}{\mathrm{d}c}=-10\left(\frac{c_{\mathrm{eq}}^{\alpha}-c_{\mathrm{eq}}^{\beta}}{2}\right)^2(c^{n}). \tag{15}$$

In equation (11), the elastic energy density $\partial F_{\mathrm{el}}(c_{ij}^{n},\mathbf{u}_{ij}^{n})/\partial c$ is discretized as

$$\begin{aligned}\frac{\partial F_{\mathrm{el}}(c_{ij}^{n},\mathbf{u}_{ij}^{n})}{\partial c}&=-K\eta(c_{ij}^{n}-c_s)\left[\frac{u_{i+1,j}-u_{i-1,j}+v_{i,j+1}-v_{i,j-1}}{2h}-\eta(c_{ij}^{n}-c_s)\right]\\&-\eta((C_{11})_{ij}^{n}+(C_{12})_{ij}^{n})\left[\frac{u_{i+1,j}-u_{i-1,j}+v_{i,j+1}-v_{i,j-1}}{2h}-2\eta(c_{ij}^{n}-c_s)\right]\\&+(C_{44}^{\mathrm{l}}-C_{44}^{0})\frac{(u_{i,j+1}-u_{i,j-1}+v_{i+1,j}-v_{i-1,j})^2}{8h^2}\\&+(C_{11}^{\mathrm{l}}-C_{11}^{0})\left[\frac{(u_{i+1,j}-u_{i-1,j})^2+(v_{i,j+1}-v_{i,j-1})^2}{8h^2}\right]\\&+(C_{12}^{\mathrm{l}}-C_{12}^{0})\frac{(u_{i+1,j}-u_{i-1,j})(v_{i,j+1}-v_{i,j-1})}{4h^2},\end{aligned}$$

where $K = C_{11}^{1} - C_{11}^{0} + C_{12}^{1} - C_{12}^{0}$ and displacement vector $\mathbf{u} = (u, v)$ satisfies equations (8) and (9). Next, we discretize equations (8) and (9) as

$$\begin{aligned}
&(C_{11})_{i+\frac{1}{2},j}(u_{i+1,j} - u_{ij}) - (C_{11})_{i-\frac{1}{2},j}(u_{ij} - u_{i-1,j}) \\
&+0.25(C_{12})_{i+1,j}(v_{i+1,j+1} - v_{i+1,j-1}) - 0.25(C_{12})_{i-1,j}(v_{i-1,j+1} - v_{i-1,j-1}) \\
&+(C_{44})_{i,j+\frac{1}{2}}(u_{i,j+1} - u_{ij}) - (C_{44})_{i,j-\frac{1}{2}}(u_{ij} - u_{ij-1}) \\
&+0.25(C_{44})_{i,j+1}(v_{i+1,j+1} - v_{i-1,j+1}) - 0.25(C_{44})_{i,j-1}(v_{i+1,j-1} - v_{i-1,j-1}) \\
&= 0.5h\eta\left[(C_{11} + C_{12})_{i+1,j}c_{i+1,j} - (C_{11} + C_{12})_{i-1,j}c_{i-1,j}\right], \\
&(C_{11})_{i,j+\frac{1}{2}}(v_{i,j+1} - v_{ij}) - (C_{11})_{i,j-\frac{1}{2}}(v_{ij} - v_{i,j-1}) \\
&+0.25(C_{12})_{i,j+1}(u_{i+1,j+1} - u_{i-1,j+1}) - 0.25(C_{12})_{i,j-1}(u_{i+1,j-1} - u_{i-1,j-1}) \\
&+(C_{44})_{i+\frac{1}{2},j}(v_{i+1,j} - v_{ij}) - (C_{44})_{i-\frac{1}{2},j}(v_{ij} - v_{i-1,j}) \\
&+0.25(C_{44})_{i+1,j}(u_{i+1,j+1} - u_{i+1,j-1}) - 0.25(C_{44})_{i-1,j}(u_{i-1,j+1} - u_{i-1,j-1}) \\
&= 0.5h\eta\left[(C_{11} + C_{12})_{i,j+1}c_{i,j+1} - (C_{11} + C_{12})_{i,j-1}c_{i,j-1}\right].
\end{aligned}$$

Here, $(C_k)_{i+\frac{1}{2},j} = \left[(C_k)_{i+1,j} + (C_k)_{ij}\right]/2$ for $k = 11$, 12, and 44.

All discrete equations are solved by multigrid method which is the efficient solver among the iterative method. For more details about multigrid method, see [27].

3. Numerical results

In this section, we perform several numerical tests. Throughout the numerical experiments, unless otherwise specified, we use the gradient energy coefficient $\epsilon = 1.2247$, the composition expansion coefficient $\eta = 0.05$, spatial step size $h = 1$, temporal step size $\Delta t = 1$ and the computational domain $\Omega = (0, 256) \times (0, 256)$. For chemical free energy function, we use $\theta_c = 1, \theta = 0.62, c_{eq}^{\alpha} = 0.053, c_{eq}^{\beta} = 0.947$ and $\delta = 0.04$. To match interfacial transition width, we scaled the logarithmic free energy as $2F_{\delta}^{\log}(c)$.

3.1. Spinodal decomposition

Figure 2 represents a phase diagram showing the binodal and spinodal lines with logarithmic function (3) and polynomial function (4). As shown in figure 2, there are three curves in the phase diagram. Among these curves, the uppermost one is known as binodal curve. The region above the binodal is stable. The other two curves are known as the spinodal curves of the logarithmic and the polynomial free energies. The curve is made by the critical points of the free energy function. The region between the binodal and spinodal curves is designated by metastable and the remaining region is called unstable [28].

To see the different evolutionary dynamics of the CH equation with the logarithmic and the polynomial free energies, we perform numerical phase separation tests with three different average concentrations $m_1 = 0.1$, $m_2 = 0.2$ and $m_3 = 0.3$ (see figure 2). For numerical simulation, we use the polynomial free energy (4) with $c_{eq}^{\alpha} = 0.053, c_{eq}^{\beta} = 0.947$ and the regularized

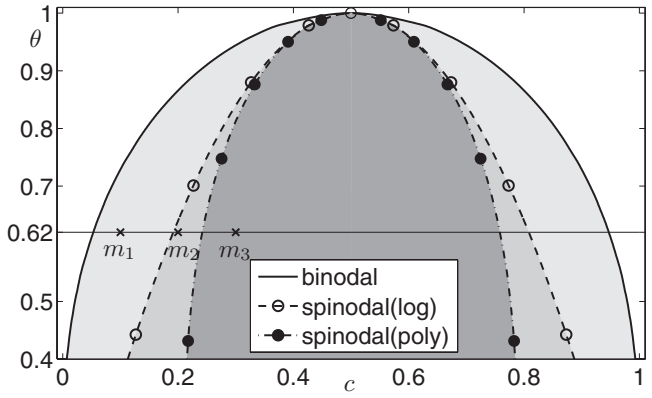

Figure 2. Phase diagram showing the binodal and spinodal lines with logarithmic and polynomial functions.

logarithmic free energy (5) with $\theta_c = 1$, $\theta = 0.62$, $\delta = 0.04$ and $\epsilon = 0.000\,625$. $\Delta t = 0.01$, $h = 1/256$ and $\Omega = (0, 1) \times (0, 1)$ are used.

Figure 3 shows the temporal evolution for solving the original CH equation without the elastic free energy term. In this test, the initial conditions are set to (*a*) $c(x, y, 0) = m_1 + 0.2\text{rand}(x, y)$, (*b*) $c(x, y, 0) = m_2 + 0.2\text{rand}(x, y)$ and (*c*) $c(x, y, 0) = m_3 + 0.2\text{rand}(x, y)$, where $\text{rand}(x, y)$ is a random number distributed uniformly in $[-1, 1]$. Here, the first column is the initial conditions. The second and the third columns are the numerical results at $t = 1$ with the logarithmic and the polynomial free energies, respectively. In figure 3(*a*), the average concentration is $m_1 = 0.1$, which is in the metastable region of both free energies. The result shows the initial perturbation was damped and the concentration became uniform. In figure 3(*b*), $m_2 = 0.2$, which is in the spinodal region of the logarithmic free energy and in the metastable region of the polynomial free energy. In this case, we can observe phase separation only with the logarithmic energy. In figure 3(*c*), $m_3 = 0.3$, which is in the spinodal region of both free energies. Both logarithmic and polynomial free energies made phase separation.

3.2. Comparison of logarithmic and polynomial free energies

Next, we include the elastic free energy term and compare results from two different bulk free energies. We take an initial condition as a circular precipitate with composition $c_{\text{eq}}^{\beta} = 0.947$ and matrix with $c_{\text{eq}}^{\alpha} = 0.053$, i.e.

$$c(x, y, 0) = \frac{c_{\text{eq}}^{\beta} - c_{\text{eq}}^{\alpha}}{2} \tanh \frac{40 - \sqrt{(x - 128)^2 + (y - 128)^2}}{2\sqrt{2}\,\epsilon} + \frac{c_{\text{eq}}^{\beta} + c_{\text{eq}}^{\alpha}}{2}. \tag{16}$$

We denote C_k^0 and C_k^1 ($k = 11,\ 12,\ 44$) as elastic constants of the precipitate and matrix phases, respectively. In this simulation, we use the following elastic constants: $C_{11}^0 = 232$, $C_{12}^0 = 153$, $C_{44}^0 = 117$, $C_{11}^1 = 204.35$, $C_{12}^1 = 180.65$ and $C_{44}^1 = 35.1$. Figures 4(*a*)–(*c*) show $c = 0.5$ level contours of the concentration field at $t = 200$, 1000 and 2000, respectively. Evolution of compositional profiles as a function of time for a soft precipitate along (*d*) the

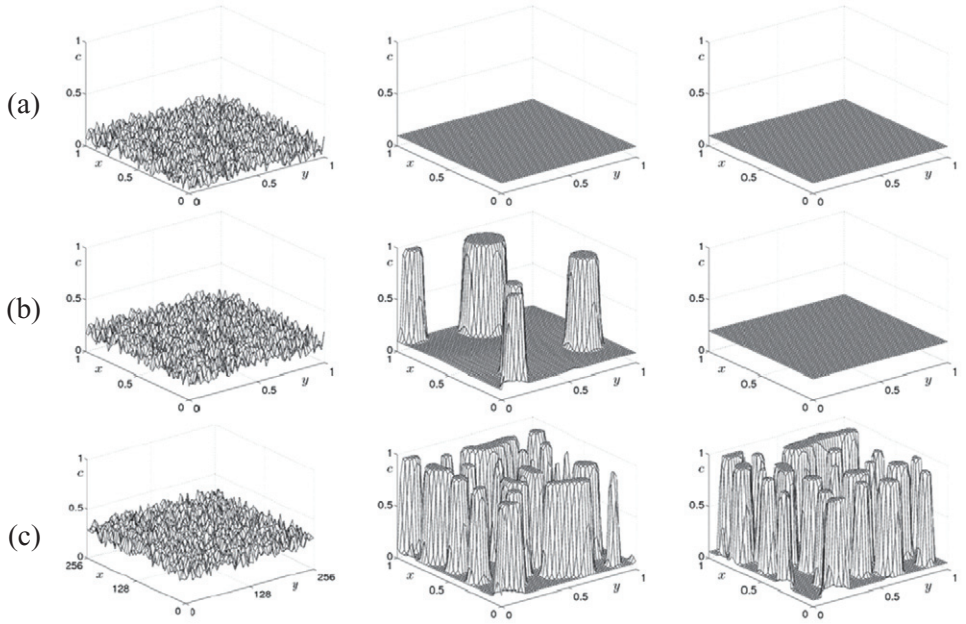

Figure 3. Temporal evolution for solving the original CH equation without the elastic free energy term. The initial conditions are (*a*) $c(x, y, 0) = m_1 + 0.2\text{rand}(x, y)$, (*b*) $c(x, y, 0) = m_2 + 0.2\text{rand}(x, y)$ and (*c*) $c(x, y, 0) = m_3 + 0.2\text{rand}(x, y)$. Here, the first column is the initial conditions. The second and the third columns are the numerical results at $t = 1$ with the logarithmic and the polynomial free energies, respectively.

x-direction at $y = 128$ and (*e*) the diagonal direction, $x = y$. The result indicates that the logarithmic free energy makes the precipitate be more elongated.

3.3. Convergence test

From now on, we will use the logarithmic free energy in the subsequent numerical experiments. In this section, we will perform a convergence test. We take the same initial condition (16). In this simulation, we use the following elastic constants: $C_{11}^0 = 232, C_{12}^0 = 153, C_{44}^0 = 117, C_{11}^1 = 204.35, C_{12}^1 = 180.65$ and $C_{44}^1 = 35.1$. Figure 5 shows $c = 0.5$ level contours at $t = 2000$ with $\Delta t = 0.1$, 1, 10 and 100. And the gray region is a contour image of $c = 0.5$ level when $\Delta t = 0.1$. We can confirm that the results converge as the time step size is refined. The results with $\Delta t = 1$ and $\Delta t = 0.1$ are almost identical.

3.4. Temporal evolutions of a soft precipitate

To verify the proposed numerical scheme, we perform the same numerical tests in [13, 29]. The shapes of a single coherent precipitate in elastically inhomogeneous systems have been studied with boundary integral method [7, 11, 12], discrete atom method [8, 9], conjugate gradient method [10] and perturbation method [13, 30]. As the first example, we investigate the shape evolution of a single precipitate and its dependence on elastic inhomogeneity. The initial condition is taken to be equation (16). And we use the following elastic constants: $C_{11}^0 = 232, C_{12}^0 = 153, C_{44}^0 = 117, C_{11}^1 = 204.35, C_{12}^1 = 180.65$ and $C_{44}^1 = 35.1$.

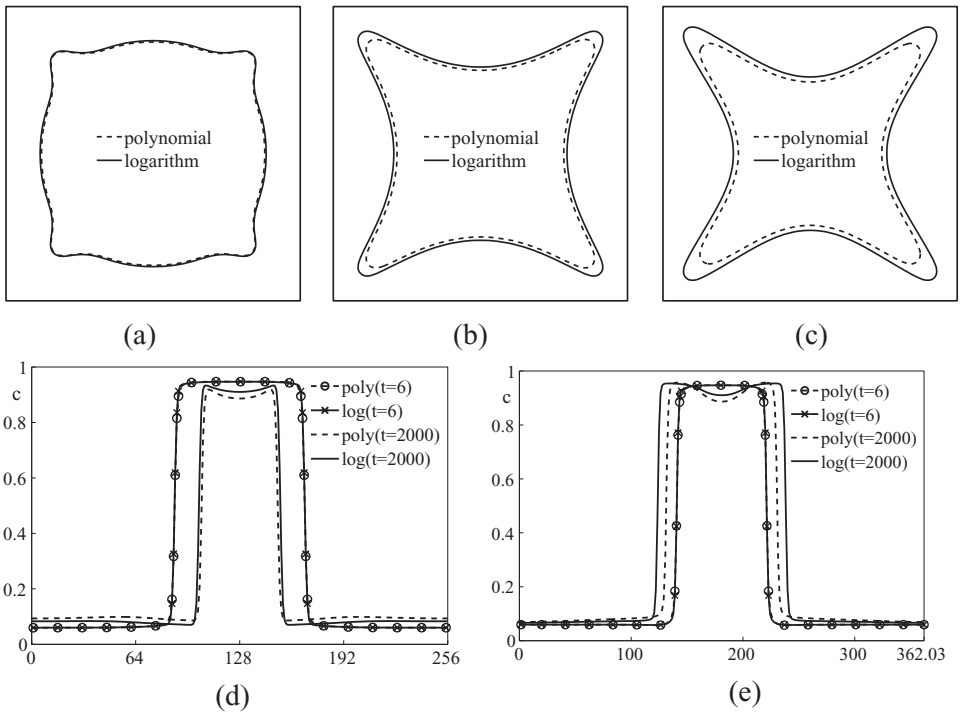

Figure 4. (*a*)–(*c*) are $c = 0.5$ level contours at $t = 200$, 1000 and 2000, respectively. Evolution of compositional profiles as a function of time for a soft precipitate along (*d*) the x-direction at $y = 128$ and (*e*) the diagonal direction, $x = y$.

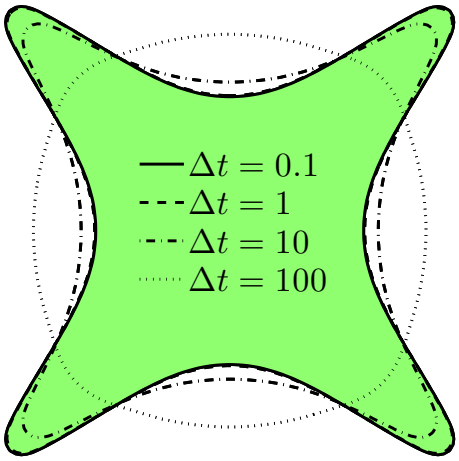

Figure 5. $c = 0.5$ level contours at $t = 2000$ with $\Delta t = 0.1$, 1, 10 and 100.

Figures 6(*a*)–(*f*) show the snapshots of a circular precipitate with shear modulus $\kappa = 0.3$ at time $t = 6$, 100, 200, 500, 1000 and 2000, respectively. And figure 6(*g*) represents the overlapped time evolution of $c(x, y)$ with the initial circle. Here, the arrow indicates the increasing time. As shown in figure 6, we can see that the initial circular shape evolves to a star shape which is cubically anisotropic as time goes on.

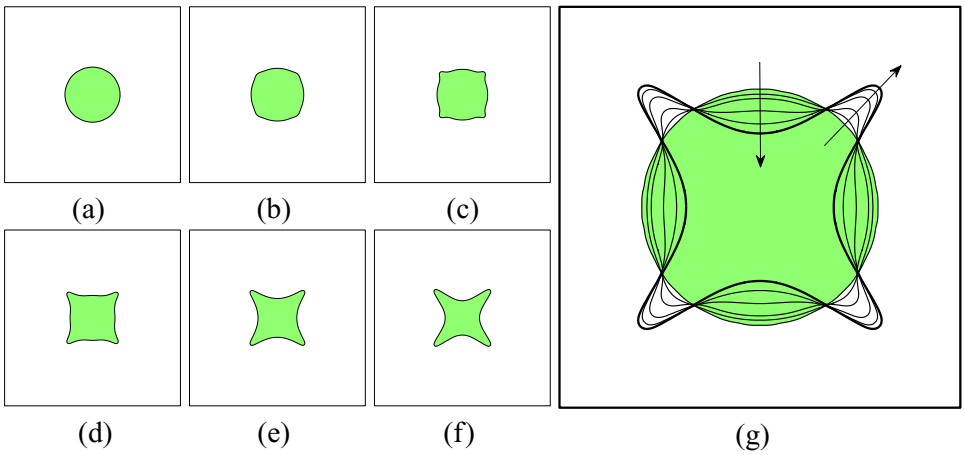

Figure 6. Temporal evolutions of a soft precipitate with shear modulus $\kappa = 0.3$. (*a*)–(*f*) Snapshots of $c(x, y)$ at time $t = 6$, 100, 200, 500, 1000 and 2000, respectively. (*g*) Overlapped evolution of $c(x, y)$ with the initial circle. Here, the arrow indicates the increasing time.

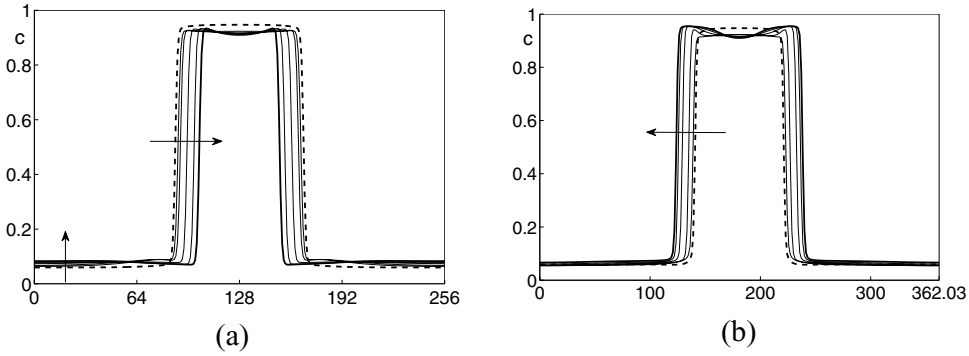

Figure 7. Evolution of compositional profiles as a function of time for a soft precipitate along (*a*) the *x*-direction and (*b*) the diagonal direction. Here, the arrow indicates the increasing time. Dashed and solid lines represent the results at $t = 6$ and $t = 2000$, respectively.

Figure 7 shows the composition $c(x, y)$ distributions along x-direction and the diagonal direction passing through the center of the precipitate with respect to time. In figure 7, solid and dashed lines represent the results at $t = 6$ and $t = 2000$, respectively. And the arrow indicates the time evolution.

3.5. Effect of elastic inhomogeneity κ

With the same initial condition (16), we investigate the effect of elastic inhomogeneity κ. We take the same elastic constants $C_{11}^0 = 232$, $C_{12}^0 = 153$ and $C_{44}^0 = 117$ as in [13, 31], which have a cubically anisotropic system. In order to show the effect of elastic inhomogeneity, we keep the same bulk modulus $B = C_{11} + C_{12}$ and the same ratio of anisotropy $\delta = 2\,C_{44}/(C_{11} - C_{12})$, while changing the ratio of shear modulus $\kappa = C_{44}^1/C_{44}^0$ in the matrix and precipitate phases, respectively [13].

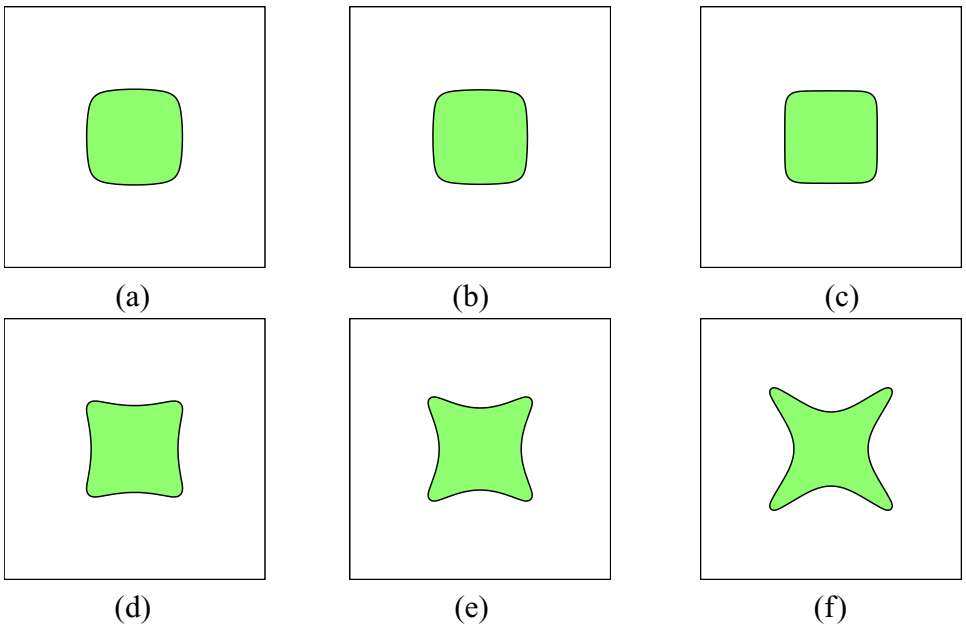

Figure 8. Morphologies of a circular precipitate with different shear modulus κ at time $t = 2000$. Here, (a)–(d) use the ratio of shear modulus $\kappa = 1.7$, 1.35, 1, 0.6 and 0.3, respectively.

Figures 8(a)–(f) show the numerical results at time $t = 2000$ with the ratio of shear modulus $\kappa = 1.7$, 1.35, 1, 0.6 and 0.3, respectively. The decrease of κ means that $C^1_{44} = \kappa C^0_{44}$, that is, the stiffness of the precipitate is less than the matrix [8, 9, 12]. Therefore, the precipitate phase is easy to deform to star shape when $\kappa < 1$ as shown in figures 8(d)–(f).

3.6. Effect of the anisotropy ratio δ

We investigate the effect of the anisotropy ratio δ. In this numerical test, we use the elastic constants $C^0_{11} = 230 + 70/\delta^M$, $C^0_{12} = 230 - 70/\delta^M$, $C^0_{44} = 70$, $C^0_{11} = 230 + 70/\delta^P$, $C^0_{12} = 230 - 70/\delta^P$ and $C^0_{44} = 70$, which are the same values as in [13]. For the numerical simulation, we use the same bulk and shear moduli, while changing the ratio of shear modulus in precipitate and matrix phases [13]. In this test, we set (δ^P, δ^M) as (1, 1), (1.14, 0.89), (1.34, 0.79), (1.63, 0.72), (2.05, 0.66) and (2.8, 0.61), respectively. And the initial state is taken to be

$$c(x, y, 0) = 0.5 + 0.1\text{rand}(x, y). \tag{17}$$

Figure 9 shows the numerical results with different anisotropy ratio δ at time $t = 2000$. As the ratio between δ^P and δ^M is getting larger, the precipitate phase becomes decomposed to several cuboid whose edges are concave [13].

3.7. Numerical stability test

The proposed numerical method is based on the unconditionally gradient stable splitting scheme [25, 26]. To show the robustness of the proposed scheme, we perform the numerical test with different time step size Δt. In this test, we set the same initial condition (17) in case of figure 9(f). In this numerical test, we use the elastic constants

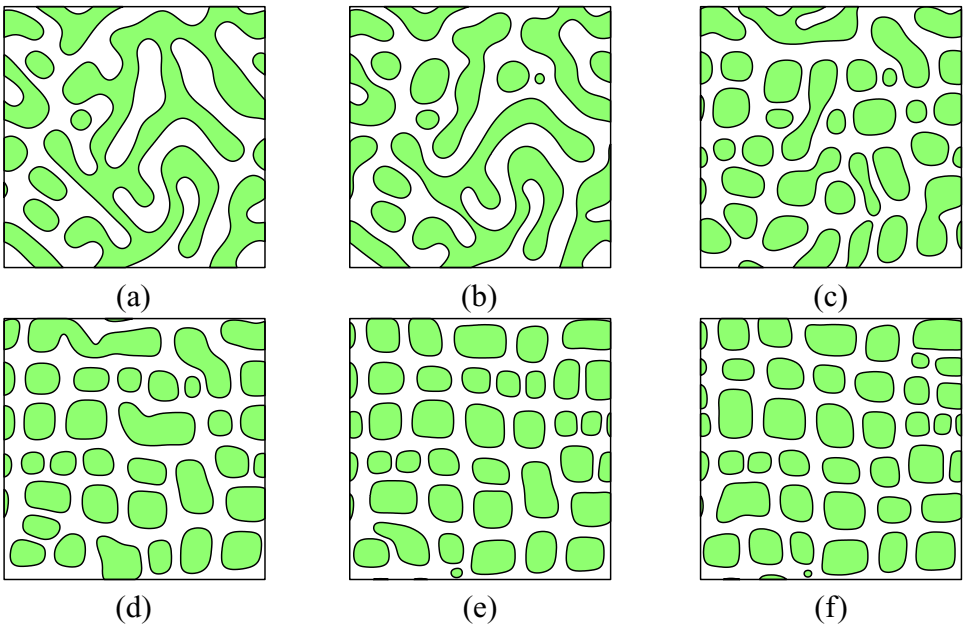

Figure 9. Morphologies of $c(x, y)$ with different ratio of elastic anisotropy (δ^P, δ^M) at time $t = 2000$: (*a*) (1, 1), (*b*) (1.14, 0.89), (*c*) (1.34, 0.79), (*d*) (1.63, 0.72), (*e*) (2.05, 0.66) and (*f*) (2.80, 0.61).

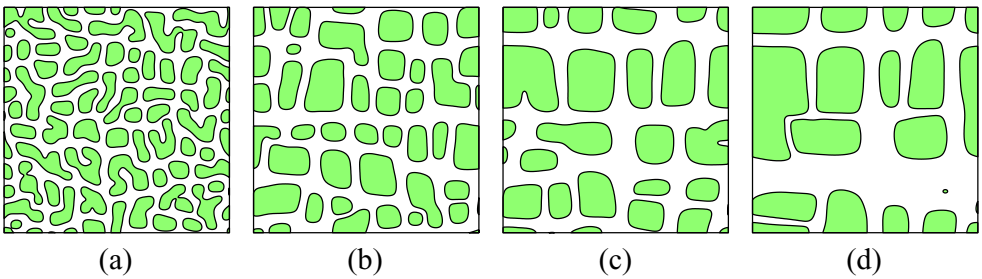

Figure 10. Numerical results after 300 iterations with (*a*) $\Delta t = 1$, (*b*) $\Delta t = 10$, (*c*) $\Delta t = 100$ and (*d*) $\Delta t = 1000$.

$C_{11}^0 = 344.7541$, $C_{12}^0 = 115.2459$, $C_{44}^0 = 70$, $C_{11}^1 = 256$, $C_{12}^1 = 205$ and $C_{44}^1 = 70$. Figures 10(*a*)–(*d*) show the numerical results after 300 iterations with $\Delta t = 1$, 10, 100 and 1000, respectively. From this test, we can confirm that our proposed numerical scheme allows the sufficiently large time step size Δt without blow-up of the numerical solution.

4. Conclusion

We proposed a fast, efficient and robust numerical method for the modified Cahn–Hilliard equation with a logarithmic free energy for microstructure evolution. Even though it is physically more appropriate to use a logarithmic free energy, a quartic polynomial approximation has been typically used for the logarithmic function due to a logarithmic singularity. In

order to overcome the singularity problem, we regularized the logarithmic function and then apply an unconditionally stable scheme to the Cahn–Hilliard part in the model. We presented computational results highlighting the different dynamic aspects from two different bulk free energy forms. We also demonstrated the robustness of the regularization of the logarithmic free energy, which implies the time-step restriction is based on accuracy and not stability.

Acknowledgments

The first author (D Jeong) was supported by Basic Science Research Program through the National Research Foundation of Korea (NRF) funded by the Ministry of Education, Science and Technology (2014R1A6A3A01009812). The corresponding author (J S Kim) was supported by the National Research Foundation of Korea(NRF) grant funded by the Korea government(MSIP) (NRF-2014R1A2A2A01003683). The authors are grateful to the reviewers whose valuable suggestions and comments significantly improved the quality of this paper.

References

[1] Zhu J, Chen L-Q and Shen J 2001 Morphological evolution during phase separation and coarsening with strong inhomogeneous elasticity *Mod. Simul. Mater. Sci. Eng.* **9** 499–511
[2] Khachaturyan A G 1983 *Theory of Structural Transformations in Solids* (New York: Wiley)
[3] Chen L-Q and Khachaturyan A G 1991 Computer simulation of structural transformations during precipitation of an ordered intermetallic phase *Acta Mater.* **39** 2533–51
[4] Chen L-Q 2002 Phase-field models for microstructure evolution *Annu. Rev. Mater. Res.* **32** 113–40
[5] Wang Y, Chen L-Q and Khachaturyan A G 1993 Kinetics of strain-induced morphological transformation in cubic alloys with a miscibility gap *Acta Metall. Mater.* **41** 279–96
[6] Yu P, Hu S Y, Chen L-Q and Du Q 2005 An iterative-perturbation scheme for treating inhomogeneous elasticity in phase-field models *J. Comput. Phys.* **208** 34–50
[7] Jou H J, Leo P H and Lowengrub J S 1997 Microstructural evolution in inhomogeneous elastic media *J. Comput. Phys.* **131** 109–48
[8] Lee J K 1996 A study on coherency strain and precipitate morphologyvia a discrete atom method *Metall. Mater. Trans.* A **27** 1449–59
[9] Lee J K 1998 Elastic stress and microstructural evolution *Mater. Trans. JIM* **39** 114–32
[10] Leo P H, Lowengrub J S and Hou H J 1998 A diffuse interface model for microsctructural evolution in elastically stressed solids *Acta Mater.* **46** 2113–30
[11] Schmidt I and Gross D 1997 The equilibrium shape of an elastically inhomogeneous inclusion *J. Mech. Phys. Solids* **45** 1521–49
[12] Schmidt I, Mueller R and Gross D 1998 The effect of elastic inhomogeneity on equilibrium and stability of a two particle morphology *Mech. Mater.* **30** 181–96
[13] Hu S Y and Chen L-Q 2001 A phase-field model for evolving microstructures with strong elastic inhomogeneity *Acta Mater.* **49** 1879–90
[14] Wise S M, Lowengrub J S, Kim J S and Johnson W C 2004 Efficient phase-field simulation of quantum dot formation in a strained heteroepitaxial film *Superlattice Microstruct.* **36** 293–304
[15] Cahn J W and Hilliard J E 1958 Free energy of a nonuniform system I: interfacial free energy *J. Chem. Phys.* **28** 258–67
[16] Cheng M and Warren J A 2007 Controlling the accuracy of unconditionally stable algorithms in the Cahn–Hilliard equation *Phys. Rev.* E **75** 017702
[17] De Mello E V L and Teixeira da Silveira Filho O 2005 Numerical study of the Cahn–Hilliard equation in one, two and three dimensions *Physics* A **347** 429–43
[18] He L and Liu Y 2009 A class of stable spectral methods for the Cahn–Hilliard equation *J. Comput. Phys.* **228** 5101–10
[19] He Y, Liu Y and Tang T 2006 On large time-stepping methods for the Cahn–Hilliard equation *Appl. Numer. Math.* **57** 616–28
[20] Kay D and Welford R 2006 A multigrid finite element solver for the Cahn–Hilliard equation *J. Comput. Phys.* **212** 288–304

[21] Sheng G, Wang T, Du Q, Wang K G, Liu Z K and Chen L-Q 2010 Coarsening kinetics of a two phase mixture with highly disparate diffusion mobility *Commun. Comput. Phys.* **8** 249–64
[22] Garcke H, Rumpf M and Weikard U 2001 The Cahn–Hilliard equation with elasticity, finite element approximation and qualitative analysis *J. Interface Free Bound.* **3** 101–18
[23] Garcke H, Maier-Paape S and Weikard U 2003 Spinodal decomposition in the presence of elastic interactions *Geometric Analysis and Nonlinear Partial Differential Equations* (Berlin: Springer) pp 603–35
[24] Barrett J W and Blowey J F 1999 Finite element approximation of the Cahn–Hilliard equation with concentration dependent mobility *Math. Comput.* **68** 487–517
[25] Eyre D J www.math.utah.edu/eyre/research/methods/stable.ps (unpublished paper)
[26] Eyre D J 1998 *Computational and Mathematical Models of Microstructural Evolution* (Warrendale: The Material Research Society)
[27] Trottenberg U, Oosterlee C and Schüller A 2001 *Multigrid* (London: Academic)
[28] Cahn J W 1961 On spinodal decomposition *Acta Metall.* **9** 795–801
[29] Hu S 2004 Phase-field models of microstructure evolution in a system with elastic inhomogeneity and defects *Doctoral Dissertation* The Pennsylvania State University
[30] Khachaturyan A G, Semenovskaya S and Tsakalakos T 1995 Elastic strain energy of inhomogeneous solids *Phys. Rev.* B **52** 15909–19
[31] Paris O, Langmanyr F, Vogl G and Fratzl P 1995 A possible criterion for slowing down of precipitate coarsening due to elastic misfit interactions *Z. Met.kd.* **86** 860–3